Proliferation drives quorum sensing of microbial products in human macrophage populations

Nadia Rajab[1], Linden J. Gearing[2,3], Ruqian Lyu[4,5], Yair D.J. Prawer[1], Paul W. Angel[1], Sean M. Grimmond[6], Andrew L. Laslett[7], Davis J. McCarthy[4,5], and Christine A. Wells[1#]

1. Centre for Stem Cell Systems, Department of Anatomy and Physiology, Faculty of Medicine, Dentistry and Health Sciences, The University of Melbourne, VIC, 3010, Australia.
2. Centre for Innate Immunity and Infectious Diseases, Hudson Institute of Medical Research, Clayton, VIC, 3168, Australia.
3. Department of Molecular and Translational Sciences, Monash University, Clayton, VIC, 3168, Australia.
4. Bioinformatics and Cellular Genomics, St Vincent's Institute of Medical Research, Fitzroy, Australia
5. Melbourne Integrative Genomics, School of Biosciences – School of Mathematics & Statistics, Faculty of Science, University of Melbourne, Melbourne, Australia
6. University of Melbourne Centre for Cancer Research, Faculty of Medicine, Dentistry and Health Sciences, The University of Melbourne, VIC, 3010, Australia.
7. Australian Regenerative Medicine Institute, Monash University, Melbourne, VIC 3800, Australia.

#Correspondence to CAW wells.c@unimelb.edu.au

Author Contributions

N.R. experimental design, data generation and analysis, writing

L.J.G. data analysis

R.L. SNP deconvolution and analysis

Y.D.J.P library preparation, data processing

P.W.A. data analysis

S.M.G experimental resources

A.L.L. experimental resources

D.M. experimental resources

C.A.W. experimental design, data analysis, writing, project funding

Conflict of Interests

NR and YDJP received training and subsidised reagents from 10X Genomics for the preparation of samples described in this manuscript. The company did not seek to influence experimental design, or interpretation of the data in this manuscript. No COI is declared for the other authors.

Funding

The project was run as part of the 10X Genomics Millenium Science Start Single Cell Fellowship to NR and YDJP. C.A.W. is funded by NHMRC Synergy grant APP1186371.

Acknowledgements

The authors thank the Genomics Platform Group at The University of Melbourne Centre for Cancer Research (UMCCR) sequencing core for sequencing of single-cell libraries, and Prof. Oliver Hofmann for computational workflows and project discussions. The authors thank Dr Catherine King (10x Genomics) and Dr Paul Gooding (Millenium Science) for their training and assistance in preparation of 10x libraries. The authors thank Dr Jarny Choi and Dr Michael Clark, University of Melbourne, for reading and commenting on the manuscript.

Abstract

Macrophages coordinate the initial host inflammatory response to tissue infection, as well as mediating the reparative phase, by producing growth factors that promote tissue repair. One model of this functional dichotomy is that peripherally recruited monocyte-derived macrophages drive acute inflammatory responses to infection, whereas tissue-resident macrophages are responsible for tissue repair. Alternatively, inflammation and repair may be inter-dependent molecular programs, such that both recruited and resident cells have equivalent capacity to contribute. Repeated exposure to pathogenic challenge results in innate tolerance, which may also alter the contributions of discrete macrophage populations to inflammation or repair. In this study a village model of tissue resident and recruited macrophages was created using induced pluripotent stem cell-derived macrophages and peripheral blood monocyte-derived macrophages, respectively. Population responses to repeated exposure to lipopolysaccharide were assessed with single-cell RNA sequencing and donors demultiplexed with Vireo. A subset of genes escaped classical tolerance programs in the iPSC, but not monocyte-derived macrophages, and this was associated with differences in their proliferative capacity. This suggests that targeting the proliferative resident macrophages would be most effective to limit inflammatory signaling.

Key words:

Macrophage, pluripotent stem cells, endotoxin tolerance, innate memory, inflammation, lipopolysaccharide

Introduction

Multiple tissue-resident macrophage subsets have been described and defined by roles that are specialized to their tissue of residency, such as bone resorption by osteoclasts[1], neural pruning by microglia[2], lipid-associated macrophages[3], stem cell licensing in bone marrow[4] and intestine[5], or iron recycling in splenic macrophages[6]. Differences between macrophage subsets have also been described in the context of ontogeny (reviewed in [7]), anatomical location, or molecular phenotype[8]. Given the diverse roles of macrophages in tissue development, homeostasis, and in host defense, there is considerable interest in understanding mechanisms that might target macrophage subsets in tissue inflammation or repair.

Functional differences between tissue-resident macrophages (TRM) and monocyte-derived macrophages (MDM) recruited in response to inflammation are controversial. In some models, such as brain, the resident macrophages (microglia) play a neuroprotective role, while recruited MDM are thought to be the inflammatory mediator[9]. In contrast, others have described diverse monocyte and macrophage subsets associated with age-related inflammation, cancer or trauma[10], as well as inflammatory phenotypes associated with differences in IRF8 signaling across these subsets[11]. If macrophages have predefined roles in infection or inflammation, then this observed heterogeneity might well be explained by mixing of ontogenically and phenotypically distinct populations, exemplified by the progression of liver disease[12]. Alternatively, if both resident and recruited macrophage populations are intrinsically heterogeneous, then quorum-sensing will lead to roles that are randomly assigned across all populations, ensuring that the capacity for inflammation and repair is available regardless of the origin of the responding macrophage[13].

This idea of quorum sensing is supported by early studies of stochasticity of macrophage responsiveness showing heterogeneity in gene expression after exposure to lipopolysaccharide (LPS). Examples of this have been described in studies showing variability of LPS responses in clones of murine RAW264.7 cells[13,14]. In the first study, subclones demonstrated varying levels of gene expression after LPS stimulation, suggesting the coexistence of

macrophage subsets that could be propagated as subpopulations. In the second study, heterogeneity in the timing of RelA recruitment to the TNF promoter in a RAW264.7 reporter line was observed after LPS stimulation, but variability between cells could also be explained by population density. These studies demonstrate that multiple mechanisms impact on the timing, duration, and amplitude of macrophage activation, even in simple models receiving a highly polarizing inflammatory signal, such as LPS.

It is obvious that, in a tissue setting, macrophages will be integrating signals from the local environment and it is difficult to deconvolute the influence of these signals from ontogeny over the course of an inflammatory event. Tissue culture models offer an opportunity to address cell-intrinsic sources of macrophage diversity. Macrophages derived from human induced pluripotent stem cells (PSCM) present new opportunities to model tissue residency and factors that shape human macrophage development and activation. PSCMs are an excellent model of tissue residency because they share molecular ontogeny with TRM [15,16] and are functionally equivalent to TRM in engraftment models in brain and lung[17]. A recent comparison of macrophage transcriptomes in our own Myeloid Atlas confirmed that PSCMs shared the transcriptional phenotype of primary TRM including tissues such as brain, joint and liver[18].

Given PSCMs offer an *in vitro* representation of tissue-resident cells, they provide a relevant experimental model to investigate sources of population heterogeneity in bacterial responses. While others[19] have shown that PSCMs recognize and respond to LPS, it is not known whether they can be tolerized on repeated exposure, which would more accurately mimic the regulatory program seen after an infection than a single high dose pathogen exposure. We were also curious to see how coordinated acute responses to LPS were across human macrophage populations, as perhaps early versus late responders within a population could explain some of the previously described heterogeneity in trained monocytes[20]. Here, we use single cell RNA-sequencing to investigate population responses to high-dose LPS activation and then re-stimulation using a coculture, or village, model of PSCMs and MDMs, as models of tissue residency versus recruited macrophages respectively.

139

140 **Results**

141 Establishing a 'village' of macrophages to assess macrophage heterogeneity at the single cell
142 level.

143 The transcriptional heterogeneity of macrophage subsets was evident even in the unstimulated
144 populations (Figure 1). The use of a village model removed population density as a possible driver
145 of heterogeneity (Figure 1A), as all the cells were exposed to the same local environment,
146 maintained in CSF-1 (C, control), or exposed to LPS for 2 hours (A, acute) or 18 hours (R, rest),
147 Tolerised (T) macrophages were acutely stimulates as per (A and R), then washed after 18hours,
148 and rested for 2 hours then restimulated for 2 hours with LPS. PSCM and MDM formed distinct
149 clusters across the time course that were not explained by fractions of undifferentiated or
150 nonresponsive cells – MDM and PSCMs share similar phenotypes of CD14+ CD16low populations
151 after several days culture in CSF1 (Figure 1B). Cells collected at each time point were barcoded
152 for demultiplexing after single cell RNA-sequencing and donor origin of the cell was determined
153 by SNP deconvolution, to confirm that the heterogeneity was not driven by donor
154 (Supplementary Figure 1A). LPS exposure was a strongly polarizing signal in the acute time
155 periods, but population heterogeneity increased in the resting and restimulated conditions
156 (Figure 1C, D, E).

157

158 PSCM expressed hallmark genes of tissue resident macrophages (Figure 1F, Supplementary Table
159 1), including transcription factors associated with terminal macrophage differentiation, such as
160 *MAF* [21], and markers of perivascular and lymphatic-associated macrophages including *CD169*/
161 *SIGLEC1*, *LYVE1* and *FOLR2* [22,23]. PSCMs were transcriptionally similar to MDM and primary TRM
162 (Supplementary Figure 1B and C) using the benchmarking tool in the Stemformatics Myeloid
163 Atlas. MDM subsets were distinguished by expression of immunoregulatory glycoproteins
164 *GPNMB*, a negative regulator of TLR signaling [24], macrophage migratory factors such as *FUCA1*,
165 as well as chemokine receptors. However, the most striking difference between MDM and PSCM

clusters was the presence of a proliferative subset of PSCM in the control, acute and tolerized conditions (Figure 1E).

The observations of ~40% of PSCM and <10% of MDM proliferating in the control condition is consistent with the CSF1 responsiveness of tissue resident vs recruited macrophages. PSCM and MDM were cultured in the presence of recombinant CSF1, which is a proliferative signal to tissue-resident macrophages and essential for the maintenance of bone marrow and circulating monocytes (reviewed in [25]). Monocytes are postmitotic cells in circulation, although a small fraction have been identified proliferative in response to CSF1[26]. Just 10% of the PSCM were proliferating by the resting or tolerized conditions (Figure 1E), consistent with a pro-survival but antiproliferative consequence of TLR signaling. Both proliferating and nonproliferating PSCM subsets expressed equivalent levels of components of the TLR4-LPS pathway, at similar levels to the MDM control subsets (Figure 2A).

<u>Proliferating PSCM escape LPS tolerance</u>.

LPS is a synchronizing signal that results in high expression of core inflammatory mediators in all cells receiving the signal. These included *TNF, IL1B, IL6, CXCL1, CXCL2, CXCL8, CXCL10, CCL3, CCL4L2*, and members of the shared interleukin/TLR signaling pathway including *NFKBIA* and *NFKB1* (Figure 2, Supplementary Table 1), and negative regulators of cytokine signaling such as *SOCS1* and *SOCS3.* These are predominantly targets of the TLR-MyD88-NF-κB pathway, demonstrating that the PSCM expressed an active TLR4 signaling cascade. After 18 hours activation, most inflammatory mediators have reached a baseline expression level in both macrophage populations. Restimulation with LPS resulted in hypo-responsiveness in both MDM and PSCM, particularly marked for *TNF* expression, and genes that are associated with TNF signaling, including *NFKB1, NAMPT, TNFAIP1, 2* and *8, CXCL2, DUSP2,* and *TNFSF9*. These data confirm that PSCM are LPS responsive and undergo NF-κB-associated tolerance to repeated LPS exposure.

193 PSCM did not completely mimic the monocyte-derived tolerance program. PSCMs but not MDMs
194 expressed growth factors on LPS restimulation, including *FLT1, PDGFA*, *VEGFA*, *CSF1*, *CSF1R, CSF2*,
195 *IL32*, *IL36,* and *TGFB1* (Figure 2 and Supplementary Table 1). Less than 50% of PSCM were
196 recruited to the acute inflammatory response mediated by the MyD88-independent/IRF-
197 dependent pathway, including *IRF1, OAS1, IFIT2* compared to over 80% of MDM (Figure 2D).
198 Review of the pathways differentially expressed by MDM compared to PSCM confirmed that the
199 Reactome IFN signaling pathway scored significantly higher across the MDM time course (Figure
200 2E). Other targets of intracellular TLR signaling were absent entirely in PSCM, including *IFNB1*,
201 which was inducible in MDM but not PSCM populations. This may have implications for
202 proliferation differences between MDM and PSCM, as CSF1R is targeted by IFNB signaling in
203 monocytes[27], and further evidences negative feedback of CSF1 signaling in MDM after LPS
204 activation.
205
206 Genes that were completely tolerized in the MDM such as *IL1B*, and chemokines such as *CCL3*
207 and *CCL7* were expressed at high levels in acute or resting PSCM, and in the restimulated
208 conditions. These genes were expressed regardless of proliferating status and are predominantly
209 targets of post-transcriptional (AU-response element) regulation, which may be a mechanism
210 that supports acute activation in a macrophage that is also dividing (Figure 2, Supplementary
211 Table 2).
212

213 The current model of LPS tolerance is that of an altered chromatin landscape where NF-κB p50
214 homodimers are stabilized by BCL3, preventing recruitment and binding of NF-κB heterodimers
215 to LPS responsive cytokines[28]. BCL3 nuclear translocation and activation is regulated by
216 proliferation[29] and is differentially regulated in PCSM but not MDM across the acute phase of the
217 LPS time course, so it is plausible that proliferation of PSCM resets the BCL3-dependant program
218 of LPS tolerance, allowing for ongoing expression of inflammatory mediators in a subpopulation
219 of cells.

220

221 **Discussion**

222 In this study we tested two models of cell-intrinsic responses to LPS, identifying proliferation as
223 a driver of macrophage heterogeneity in a minor subset of the MDM, whereas the proliferative
224 subset represented about half of the PSCM population. Endotoxin tolerance in restimulated
225 macrophages took two forms – either in the degree of induction of an inflammatory gene on re-
226 stimulation with LPS or in the proportion of cells capable of expression of an inflammatory
227 mediator. It was the 18 hour-stimulated and restimulated PSCM groups that continued to express
228 cytokines, such as *IL1B*, and chemokines at a high level, possibly because these escaped tolerance
229 in the cells proliferating on first exposure to LPS. TRM have the capacity to self-renew[30]. This
230 homeostatic self-sufficiency of TRM enables the population to be maintained without requiring
231 constant influx of monocytes (Figure 3).

232 Prior exposure to a TLR ligand causes hypo-responsiveness of macrophage populations to
233 subsequent stimulations, and LPS/TLR4 drives the largest cohort of tolerized genes[31]. This so-
234 called endotoxin tolerance is regulated by recruitment and stabilization of NF-κB p50 to
235 inflammatory gene promoters, preventing engagement with the transcriptional machinery and
236 silencing the locus[28]. Likewise, prior exposure to low dose pathogenic signals, cytokines, or
237 apoptotic cells can induce 'trained' responses in innate immune cells, even days after the initial
238 exposure (reviewed in [32]). While a key difference between the monocyte-derived MDM and
239 laboratory-derived PSCM is the possibility of prior pathogen exposure in monocytes or
240 precursors[20], we did not observe any evidence of so-called inflammatory macrophage
241 signatures in the naïve MDM in this study. However, expression of IFN-related pathways in
242 acutely activated MDM is consistent with 'training' of MYD88-independent signaling in the
243 MDM rather than PSCM. Activation of IRF-related pathways appears to be part of the
244 monocyte-macrophage transition[33], but was not recapitulated in the iPSC-derivation protocols.

245 The experimental design of our macrophage village tested whether LPS tolerance is a
246 consequence of reduced numbers of cells responding to repeated LPS stimulation, or whether
247 NF-κB target genes in the population are uniformly silenced. We observed maintenance of
248 expression of a range of tolerizeable genes in PSCM 18 hour and re-stimulated groups.

249 Examples of this can be seen in PSCMs through several chemokine and inflammatory genes,
250 including *IL1B*, *CCL4L2, CCL3* and *IL6* expression, suggesting that in a subset of responsive cells,
251 LPS tolerance had been evaded. Genes previously shown to be stochastically expressed in
252 mouse RAW264.7 cells included *IL6* and *TNF*, with observations that *IL6* was expressed by all
253 RAW264 clones and *TNF* only expressed by 72% of them[13,14]. Similarly, we observed that *TNF*
254 was only expressed in about 75% of human PSCMs, but in 98% of MDMs after acute stimulation
255 with LPS. *IL6* was inducible at very low levels and in few cells in both *in vitro* human
256 macrophage models. We also observed proliferative differences between MDM as a model of
257 recruited and PSCM as a model of resident-tissue macrophages, consistent with the Muldoon
258 model of proliferative-dependent quorum licensing[13]. We hypothesize that the proliferation of
259 resident macrophages ensure that some subsets can evade tolerizing signals to remain
260 responsive to persistent infection and may therefore be the preferred target for persistent
261 inflammation.

262

263 **Experimental Procedures**

264 Cell lines and ethics approvals

265 Human macrophage derivation was carried out in accordance with The University of Melbourne
266 ethics committee HREC (approvals 1851831, 1646608). Monocytes were isolated from three
267 buffy coats, obtained from the Australian Red Cross Blood Service.

268 Human pluripotent stem cells (hPSCs) used were: PB001.1 obtained from the Stem Cell Core
269 Facility at the Murdoch Children's Research Institute (hPSCreg ID: MCRIi001- A [34]); HDF51
270 (CVCL_UF42) was kindly provided to Dr Andrew Laslett by Prof. Jeanne Loring (The Scripps
271 Research Institute, CA, USA); KOLF2 (Wellcome Trust Sanger Institute; hPSCreg ID: WTSIi018-B)
272 cells were kindly provided by Prof. Paul Hertzog (Hudson Institute of Medical Research).

273 Pluripotent Stem Cell Differentiation

274 Human pluripotent stem cells were differentiated into macrophages based on protocol described
275 by [18]. Modifications were as follows: embryoid bodies were kept in rotational cultures without

276 transference to Matrigel plates for adherence, and progenitors collected from week 2 in RPMI-
277 1640 containing L-Glutamine (Life Technologies), 10% Fetal Bovine Serum and 100ng/mL CSF1
278 for macrophage differentiation (see macrophage differentiation).

279 Peripheral Blood Monocyte Isolation

280 Buffy Coat was diluted with PBS at a 1:3 dilution and underlayed with Histopaque®-1077 (Sigma-
281 Aldrich), centrifuged at 350g for 30 minutes at 24°C with no brake. Peripheral blood mononuclear
282 cells (PBMCs) were isolated from the interphase and washed twice by using MACS buffer with
283 0.5% heat inactivated Fetal Bovine Serum (FBS) and 2mM EDTA (Invitrogen™ UltraPure™ 0.5M
284 EDTA) and centrifuging at 400g for 5 minutes at 4°C, then resuspended in 40µl MACS buffer per
285 10^7 cells. Monocytes were positively selected using Human CD14 MicroBeads (Miltenyi Biotec)
286 and LS Columns, and then used for macrophage differentiation (see below). A cell count and
287 viability were determined using 0.4% Gibco™ Trypan Blue using a hemocytometer.
288

289 Macrophage differentiation

290 Monocytes or iPSC-derived myeloid progenitor cells were cultured in tissue-culture treated 6-
291 well plates. Cells were cultured in RPMI-1640 medium containing L-Glutamine (Life Technologies)
292 with 10% Fetal Bovine Serum and 100ng/ml recombinant Human M-CSF (R&D Systems) for 4
293 days.

294 Flow Cytometry

295 Cells were prepared for flow cytometry by first performing a blocking step with 5µl mouse serum
296 (Sigma-Aldrich) then cells were resuspended in FACS Buffer containing 0.5% Bovine Serum
297 Albumin (Sigma-Aldrich) in Hanks Balanced Salt Solution (no calcium, no magnesium, no phenol
298 red) (Thermo Fisher Scientific) and incubated with antibodies (see Table 1). Cell viability was
299 determined using 7-AAD (BioLegend) or PI staining solution (Invitrogen eBioscience). Gating was
300 performed based on Fluorescence Minus One. Isotypes were included as a control (Table 1).
301 Compensation was carried out by generating a matrix using compensation beads (BD™

302 CompBead Plus; Anti- 79 mouse Ig, κ). Cell analysis was carried out on a CytoFLEX S flow
303 cytometer (Beckman Coulter) using CytExpert acquisition software. Post-acquisition analysis was
304 performed with FCS Express 7 flow cytometry software.

305 Stimulation assay

306 100,000 cells of CD14+ HDF51-, PB001.1- and KOLF2-derived progenitors, or primary CD14+
307 monocytes from 3 different donors, were pooled then seeded into 6-well dishes in Gibco™
308 RPMI-1640 media (Thermo Fisher Scientific) with 10% heat inactivated FBS (Thermo Fisher
309 Scientific) and 100ng/ml M-CSF (R&D Systems). On day 4, media was changed, and cells left to
310 settle for 2 hours before stimulating with 10ng/mL LPS. After 18 hours, tolerance wells were
311 washed twice with Gibco™ PBS (Ca2+Mg2+ free; Thermo Fisher Scientific) before fresh media
312 was added and cells left to settle for 2 hours and re-stimulated with 10ng/mL LPS for 2 hours.
313 Cells were washed with Gibco™ PBS (Ca2+Mg2+ free; Thermo Fisher Scientific) before
314 incubating with macrophage cell release for 5 minutes at 37°C and collected in media,
315 centrifuged at 350g for 5 minutes and resuspended and put through a Flowmi™ strainer (before
316 cell counts were carried out for sample preparation, see 10x Illumina Single Cell Library
317 Preparation and RNA Sequencing).

318 10x Illumina Single Cell Library Preparation and RNA Sequencing

319 Single cell RNA-sequencing libraries were prepared using the Chromium Next GEM Single Cell 5'
320 v2 (Dual Index) protocol as per manufacturer's instructions. Cell suspensions were prepared for
321 a target recovery of 6000 cells per sample. Libraries were quality checked and quantified using
322 the Agilent Tapestation D5000 High Sensitivity Tape. Two sequencing runs were performed using
323 Novaseq6000 at University of Melbourne Centre for Cancer Research. Data processing and
324 merging of sequencing runs were carried out through CellRanger v6.0.2 pipeline to generate files
325 for analysis. Downstream analysis was carried out using Seurat package v4.0.5 [35].

326 Donor Deconvolution

327 The raw number of reads that were associated with each barcode were counted, and only cells
328 with more than 2000 reads associated were kept for further analysis. We applied cellSNP-lite

329 (with options: --minMAF 0.1, --minCOUNT 5)[36] for getting the allele counts for the list of
330 common SNPs in the population identified from the 1000 Genome Project[37]. We subsequently
331 applied Vireo[38] for demultiplexing the cell barcodes into 3 donors or cell lines used for each
332 sample. The same donors were then matched by their genotype similarity (Supplementary
333 Figure 1).

334

335 Differential gene expression analysis

336 A pseudo-bulk approach was used to identify differentially expressed genes[39]. The gene counts
337 in cells for each donor were aggregated to form bulk samples, and we applied differential
338 expression analysis using methods designed for bulk RNA-seq[40,41]. Briefly, 24 bulk samples were
339 created after summing gene counts for 3 donors in each time point, and lowly expressed genes
340 were filtered out. The gene counts for all samples were then normalized using TMM (trimmed
341 mean of M-values) [40]. Differential genes were identified by contrasting samples between
342 sample conditions, and the final list of DE genes in each contrasting group were obtained by the
343 "treat" method with log(2) fold change > 1[42].

344 Gene Set and Pathway Enrichment Analysis and ARE Motif Analysis

345 AU-rich element motifs were evaluated using the ARE motif database [43]. The search space was
346 restricted to 3'UTR motifs. Gene Set Enrichment Analysis (GSEA) was performed using the
347 MSigDB Hallmark gene sets [44]. Pathway enrichment used InnateDB [45] or Reactome [46] on
348 upregulated genes ≥1.5 Log2FC and p.value ≤0.05. Interferon module scores were calculated
349 with the Seurat function AddModuleScore using the Reactome interferon signaling pathway
350 gene set, obtained from the msigdbr package. Bar plots showing the average expression of
351 example genes were derived from the output of the Seurat DotPlot, taking the percentage of
352 cells per group expressing each gene of interest (bar height) and the unscaled average
353 expression per group (colour).

354 Data and code availability

355 Single cell sequencing data are available through (GSE210175). Code used for analysis is available
356 at:
357
358 https://github.com/wellslab/invitrosinglecell/blob/main/Analysiscode.R

359 **References**

360 1. Felix, R., Cecchini, M. G. & Fleisch, H. Macrophage colony stimulating factor restores in vivo
361 bone resorption in the op/op osteopetrotic mouse. *Endocrinology* **127**, 2592–2594 (1990).
362 2. Badimon, A. *et al.* Negative feedback control of neuronal activity by microglia. *Nature* **586**,
363 417–423 (2020).
364 3. Cox, N. *et al.* Diet-regulated production of PDGFcc by macrophages controls energy storage.
365 *Science* **373**, eabe9383 (2021).
366 4. Wattrus, S. J. *et al.* Quality assurance of hematopoietic stem cells by macrophages
367 determines stem cell clonality. *Science* **377**, 1413–1419 (2022).
368 5. Jardé, T. *et al.* Mesenchymal Niche-Derived Neuregulin-1 Drives Intestinal Stem Cell
369 Proliferation and Regeneration of Damaged Epithelium. *Cell Stem Cell* **27**, 646-662.e7
370 (2020).
371 6. Soe-Lin, S. *et al.* Nramp1 promotes efficient macrophage recycling of iron following
372 erythrophagocytosis in vivo. *Proc Natl Acad Sci U S A* **106**, 5960–5965 (2009).
373 7. Lee, C. Z. W. & Ginhoux, F. Biology of resident tissue macrophages. *Development* **149**,
374 dev200270 (2022).
375 8. Mulder, K. *et al.* Cross-tissue single-cell landscape of human monocytes and macrophages in
376 health and disease. *Immunity* **54**, 1883-1900.e5 (2021).

377 9. Silvin, A. *et al.* Dual ontogeny of disease-associated microglia and disease inflammatory
378 macrophages in aging and neurodegeneration. *Immunity* **55**, 1448-1465.e6 (2022).
379 10. Young, A. M. H. *et al.* A map of transcriptional heterogeneity and regulatory variation in
380 human microglia. *Nat Genet* **53**, 861–868 (2021).
381 11. Zhou, Y. *et al.* Human and mouse single-nucleus transcriptomics reveal TREM2-dependent
382 and TREM2-independent cellular responses in Alzheimer's disease. *Nat Med* **26**, 131–142
383 (2020).
384 12. Daemen, S. *et al.* Dynamic Shifts in the Composition of Resident and Recruited
385 Macrophages Influence Tissue Remodeling in NASH. *Cell Reports* **34**, 108626 (2021).
386 13. Muldoon, J. J., Chuang, Y., Bagheri, N. & Leonard, J. N. Macrophages employ quorum
387 licensing to regulate collective activation. *Nat Commun* **11**, 878 (2020).
388 14. Ravasi, T. *et al.* Generation of Diversity in the Innate Immune System: Macrophage
389 Heterogeneity Arises from Gene-Autonomous Transcriptional Probability of Individual
390 Inducible Genes. *J Immunol* **168**, 44–50 (2002).
391 15. Buchrieser, J., James, W. & Moore, M. D. Human Induced Pluripotent Stem Cell-Derived
392 Macrophages Share Ontogeny with MYB-Independent Tissue-Resident Macrophages. *Stem*
393 *Cell Reports* **8**, 334–345 (2017).
394 16. Calvanese, V. *et al.* Mapping human haematopoietic stem cells from haemogenic
395 endothelium to birth. *Nature* **604**, 534–540 (2022).
396 17. Takata, K. *et al.* Induced-Pluripotent-Stem-Cell-Derived Primitive Macrophages Provide a
397 Platform for Modeling Tissue-Resident Macrophage Differentiation and Function. *Immunity*
398 **52**, 417–418 (2020).

399 18. Rajab, N. *et al.* An integrated analysis of human myeloid cells identifies gaps in in vitro
400 models of in vivo biology. *Stem Cell Reports* **16**, 1629–1643 (2021).
401 19. Alasoo, K. *et al.* Transcriptional profiling of macrophages derived from monocytes and iPS
402 cells identifies a conserved response to LPS and novel alternative transcription. *Sci Rep* **5**,
403 12524 (2015).
404 20. Zhang, B. *et al.* Single-cell RNA sequencing reveals induction of distinct trained-immunity
405 programs in human monocytes. *Journal of Clinical Investigation* **132**, e147719 (2022).
406 21. Lavin, Y. *et al.* Tissue-Resident Macrophage Enhancer Landscapes Are Shaped by the Local
407 Microenvironment. *Cell* **159**, 1312–1326 (2014).
408 22. Moura Silva, H. *et al.* c-MAF–dependent perivascular macrophages regulate diet-induced
409 metabolic syndrome. *Sci. Immunol.* **6**, eabg7506 (2021).
410 23. Dick, S. A. *et al.* Three tissue resident macrophage subsets coexist across organs with
411 conserved origins and life cycles. *Sci. Immunol.* **7**, eabf7777 (2022).
412 24. Ripoll, V. M., Irvine, K. M., Ravasi, T., Sweet, M. J. & Hume, D. A. *Gpnmb* Is Induced in
413 Macrophages by IFN-γ and Lipopolysaccharide and Acts as a Feedback Regulator of
414 Proinflammatory Responses. *J Immunol* **178**, 6557–6566 (2007).
415 25. Sehgal, A., Irvine, K. M. & Hume, D. A. Functions of macrophage colony-stimulating factor
416 (CSF1) in development, homeostasis, and tissue repair. *Seminars in Immunology* **54**, 101509
417 (2021).
418 26. Clanchy, F. I. L. Detection and properties of the human proliferative monocyte
419 subpopulation. *Journal of Leukocyte Biology* **79**, 757–766 (2006).

420 27. Tong, Y. *et al.* Concomitant type I IFN and M-CSF signaling reprograms monocyte
421 differentiation and drives pro-tumoral arginase production. *EBioMedicine* **39**, 132–144
422 (2019).
423 28. Carmody, R. J., Ruan, Q., Palmer, S., Hilliard, B. & Chen, Y. H. Negative Regulation of Toll-
424 Like Receptor Signaling by NF-κB p50 Ubiquitination Blockade. *Science* **317**, 675–678 (2007).
425 29. Zhang, M. Y., Harhaj, E. W., Bell, L., Sun, S. C. & Miller, B. A. Bcl-3 expression and nuclear
426 translocation are induced by granulocyte-macrophage colony-stimulating factor and
427 erythropoietin in proliferating human erythroid precursors. *Blood* **92**, 1225–1234 (1998).
428 30. Hashimoto, D. *et al.* Tissue-Resident Macrophages Self-Maintain Locally throughout Adult
429 Life with Minimal Contribution from Circulating Monocytes. *Immunity* **38**, 792–804 (2013).
430 31. Butcher, S. K., O'Carroll, C. E., Wells, C. A. & Carmody, R. J. Toll-Like Receptors Drive Specific
431 Patterns of Tolerance and Training on Restimulation of Macrophages. *Front. Immunol.* **9**,
432 933 (2018).
433 32. Divangahi, M. *et al.* Trained immunity, tolerance, priming and differentiation: distinct
434 immunological processes. *Nat Immunol* **22**, 2–6 (2021).
435 33. Song, R. *et al.* IRF1 governs the differential interferon-stimulated gene responses in human
436 monocytes and macrophages by regulating chromatin accessibility. *Cell Reports* **34**, 108891
437 (2021).
438 34. Vlahos, K. *et al.* Generation of iPSC lines from peripheral blood mononuclear cells from 5
439 healthy adults. *Stem Cell Research* **34**, 101380 (2019).
440 35. Hao, Y. *et al.* Integrated analysis of multimodal single-cell data. *Cell* **184**, 3573-3587.e29
441 (2021).

442 36. Huang, X. & Huang, Y. Cellsnp-lite: an efficient tool for genotyping single cells.
443 *Bioinformatics* **37**, 4569–4571 (2021).
444 37. The 1000 Genomes Project Consortium *et al.* A global reference for human genetic
445 variation. *Nature* **526**, 68–74 (2015).
446 38. Huang, Y., McCarthy, D. J. & Stegle, O. Vireo: Bayesian demultiplexing of pooled single-cell
447 RNA-seq data without genotype reference. *Genome Biol* **20**, 273 (2019).
448 39. Law, C. W. *et al.* RNA-seq analysis is easy as 1-2-3 with limma, Glimma and edgeR. *F1000Res*
449 **5**, 1408 (2018).
450 40. Robinson, M. D., McCarthy, D. J. & Smyth, G. K. edgeR: a Bioconductor package for
451 differential expression analysis of digital gene expression data. *Bioinformatics* **26**, 139–140
452 (2010).
453 41. Ritchie, M. E. *et al.* limma powers differential expression analyses for RNA-sequencing and
454 microarray studies. *Nucleic Acids Res* **43**, e47 (2015).
455 42. McCarthy, D. J. & Smyth, G. K. Testing significance relative to a fold-change threshold is a
456 TREAT. *Bioinformatics* **25**, 765–771 (2009).
457 43. Bakheet, T., Hitti, E. & Khabar, K. S. A. ARED-Plus: an updated and expanded database of
458 AU-rich element-containing mRNAs and pre-mRNAs. *Nucleic Acids Research* **46**, D218–D220
459 (2018).
460 44. Liberzon, A. *et al.* The Molecular Signatures Database Hallmark Gene Set Collection. *Cell*
461 *Systems* **1**, 417–425 (2015).
462 45. Breuer, K. *et al.* InnateDB: systems biology of innate immunity and beyond—recent updates
463 and continuing curation. *Nucleic Acids Research* **41**, D1228–D1233 (2013).

464 46. Gillespie, M. *et al.* The reactome pathway knowledgebase 2022. *Nucleic Acids Research* **50**,

465 D687–D692 (2022).

466

467

468

469 **Tables**

Table 1 : Flow Cytometry Antibodies		
Marker	Antibody	Isotype control
CD14	Brilliant Violet 421™ anti-human CD14 Antibody (BioLegend; Cat. No. 325628)	Brilliant Violet 421™ Mouse IgG1, κ Isotype Ctrl Antibody (BioLegend: Cat. No. 400157)
CD16	Brilliant Violet 605™ anti-human CD16 Antibody (BioLegend: Cat. No. 302040)	Brilliant Violet 605™ Mouse IgG1, κ Isotype Ctrl Antibody (BioLegend: Cat. No. 400161)
CD45	APC anti-human CD45 Antibody (BioLegend: Cat. No. 368512)	APC Mouse IgG1, κ Isotype Ctrl (FC) Antibody (BioLegend: Cat. No. 400121)
CD11b	Brilliant Violet 711™ anti-human CD11b Antibody (BioLegend: Cat. No. 301344)	Brilliant Violet 711™ Mouse IgG1, κ Isotype Ctrl Antibody (BioLegend: Cat. No. 400167)
HLA-DR	Alexa Fluor® 488 anti-human HLA-DR Antibody (BioLegend: Cat. No. 307619)	Alexa Fluor® 488 Mouse IgG2a, κ Isotype Ctrl Antibody (BioLegend: Cat. No. 400233)

470

471

Figure 1 Proliferation drives macrophage heterogeneity in a village-in-a-dish model of repeated bacterial stimulation. (1A) Schematic of experimental design, including design of village coculture model for 3 MDM donors or 3 PSCM lines. Time course for LPS stimulation and multiplexed single cell library preparation. (1B) Representative surface expression of macrophage markers in MDM and PSCM measured by flow cytometry. Isotype control antibody staining (pink), signal (blue). (1C) Uniform Manifold Approximation and Projection (UMAP) of Seurat clusters (resolution 0.9) (1D) Seurat cluster group (columns) by sample barcode (rows). Groups are colour-coded according to (C) and labelled according to time point (C control, A acute, R 18 hours, T tolerance) and numbered from highest to lowest cell number per group. (1E) Genes that discriminated proliferating-cell clusters across LPS stimulation time course. Stacked bar plots indicate the proportion of proliferating-cell clusters (shaded bars) per barcode group. (1F) Key discriminating markers between UMAP clusters. Heat map of top genes (avg. Log2FC) in each subcluster. Legend denotes high (red) to low (blue) expression. See also Supplementary Figure 1, Supplementary Tables 1 and 2.

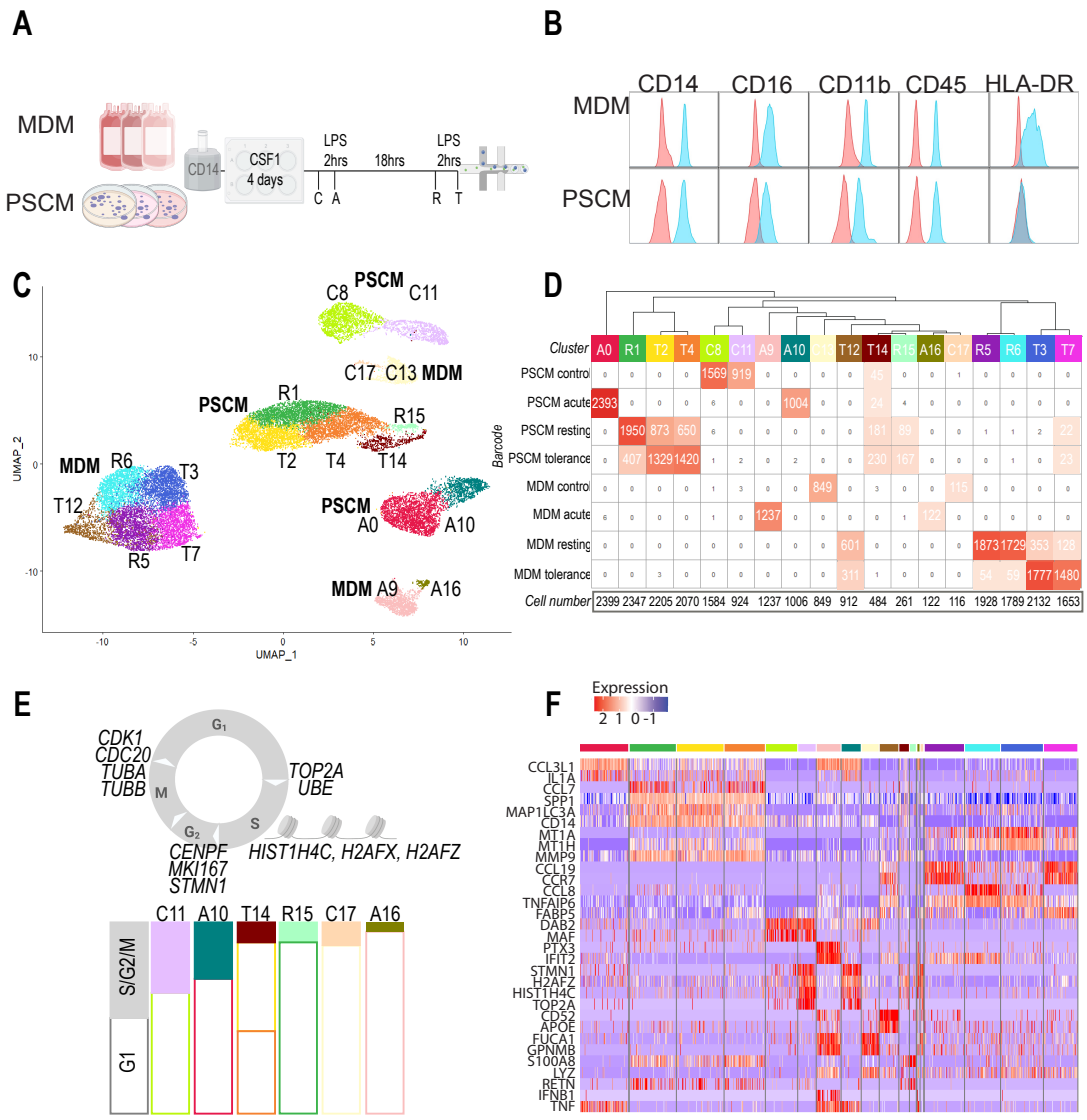

487 **Figure 2 Inflammatory gene expression varied by the proportion of cells recruited to the**
488 **inflammatory phenotype, as well as average gene expression per cell**. (2A) Schematic of the TLR
489 pathway and average expression of pathway members in unstimulated PSCM and MDM
490 populations. Bar plots coloured by cluster members (MDM Cluster C13, C17; PSCM clusters C8,
491 C11: see Figure 1C) to evaluate average expression in proliferating and nonproliferating control
492 clusters. (2B) Venn diagram of LPS-inducible genes after 2 hours (selected by Log2FC. > 1.5, Adj.
493 p value <0.05). P-values on graph indicate InnateDB pathway over-representation (Fishers exact
494 test). (2C) Percentage of cells per cluster expressing six representative targets of TLR4-LPS
495 stimulation. (2D) Percentage of cells per cluster expressing six representative targets of IRF
496 (MyD88-independent) stimulation. (2E) Seurat module scores of the Reactome Interferon
497 signaling pathway. Averaged cell score shown. (2F) Growth factor signaling persists in PSCM but
498 not MDM. Percentage of cells per cluster expressing four representative reparative factors. For
499 all bar plots, gene expression (average CPM / cell) indicated by colour where dark blue indicates
500 highest expression, light for lowest expression.

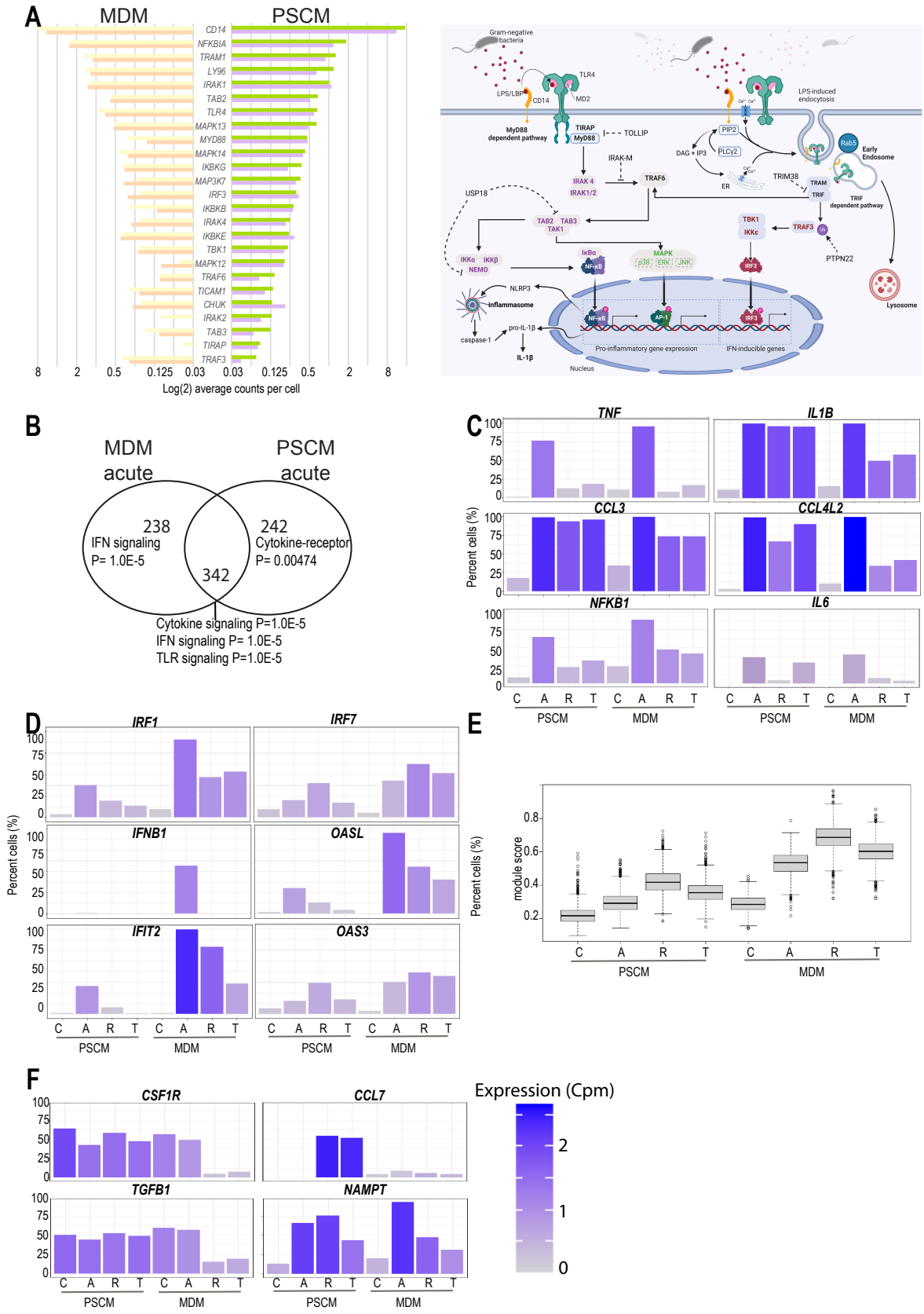
A
MDM
PSCM
CD14
NFKBIA
TRAM1
LY96
IRAK1
TAB2
TLR4
MAPK13
MYD88
MAPK14
IKBKG
MAP3K7
IRF3
IKBKB
IRAK4
IKBKE
TBK1
MAPK12
TRAF6
TICAM1
CHUK
IRAK2
TAB3
TIRAP
TRAF3
8 2 0.5 0.125 0.03 0.03 0.125 0.5 2 8
Log(2) average counts per cell
Gram-negative bacteria
LPS/LBP
CD14
TLR4
MD2
MyD88 dependent pathway
TIRAP
MyD88
TOLLIP
IRAK-M
IRAK 4
IRAK1/2
TRAF6
USP18
TAB2 TAB3
TAK1
IKKα IKKβ
NEMO
IκBα
NFκB
MAPK
p38 ERK JNK
NLRP3
inflammasome
caspase-1
pro-IL-1β
IL-1β
Nucleus
Pro-inflammatory gene expression
IFN-inducible genes
LPS-induced endocytosis
PIP2
PLCγ2
DAG + IP3
ER
TRIM38
TRAM
TRIF
TRIF dependent pathway
Rab5
Early Endosome
TBK1
IKKε
TRAF3
PTPN22
IRF3
Lysosome
B
MDM acute
PSCM acute
238
IFN signaling
P= 1.0E-5
342
242
Cytokine-receptor
P= 0.00474
Cytokine signaling P=1.0E-5
IFN signaling P= 1.0E-5
TLR signaling P=1.0E-5
C
TNF
IL1B
CCL3
CCL4L2
NFKB1
IL6
Percent cells (%)
C A R T C A R T
PSCM MDM
D
IRF1
IRF7
IFNB1
OASL
IFIT2
OAS3
Percent cells (%)
C A R T C A R T C A R T C A R T
PSCM MDM PSCM MDM
E
module score
Percent cells (%)
C A R T C A R T
PSCM MDM
F
CSF1R
CCL7
TGFB1
NAMPT
C A R T C A R T C A R T C A R T
PSCM MDM PSCM MDM
Expression (Cpm)
2
1
0

501

502 **Figure 3 Cartoon of two macrophage populations describing escape from endotoxin tolerance**

503 **in subpopulations that are proliferating**. Created in BioRender.

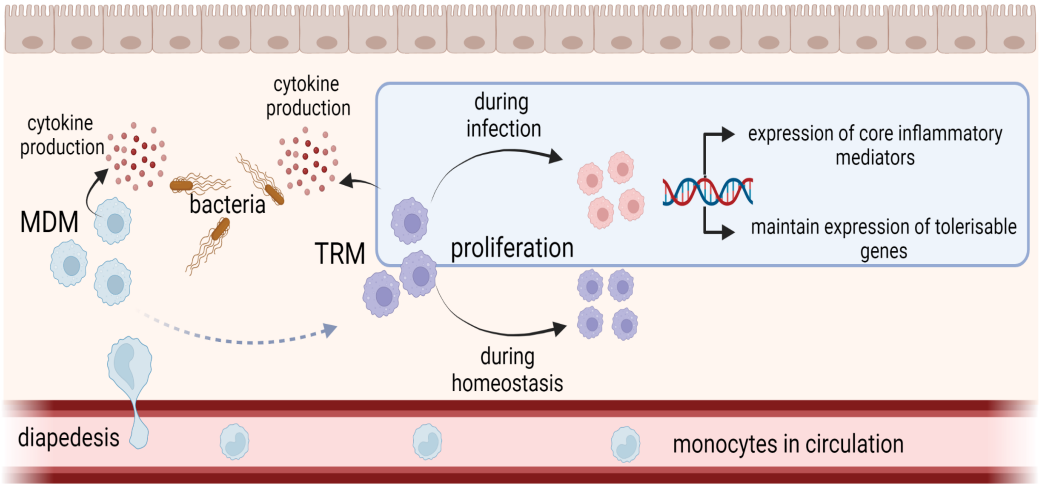

504

505

506

Supplementary Figure 1: Quality assessment of RNAseq libraries. A: donor contributions to PSCM or MDM sequencing libraries. B: Correlation of sequencing tags labelled by experimental condition (barcode) or donor ID. C: Screenshot of projection of PSCM and MDM libraries onto the Stemformatics Myeloid atlas, and Cabyara analysis of most similar reference atlas samples.

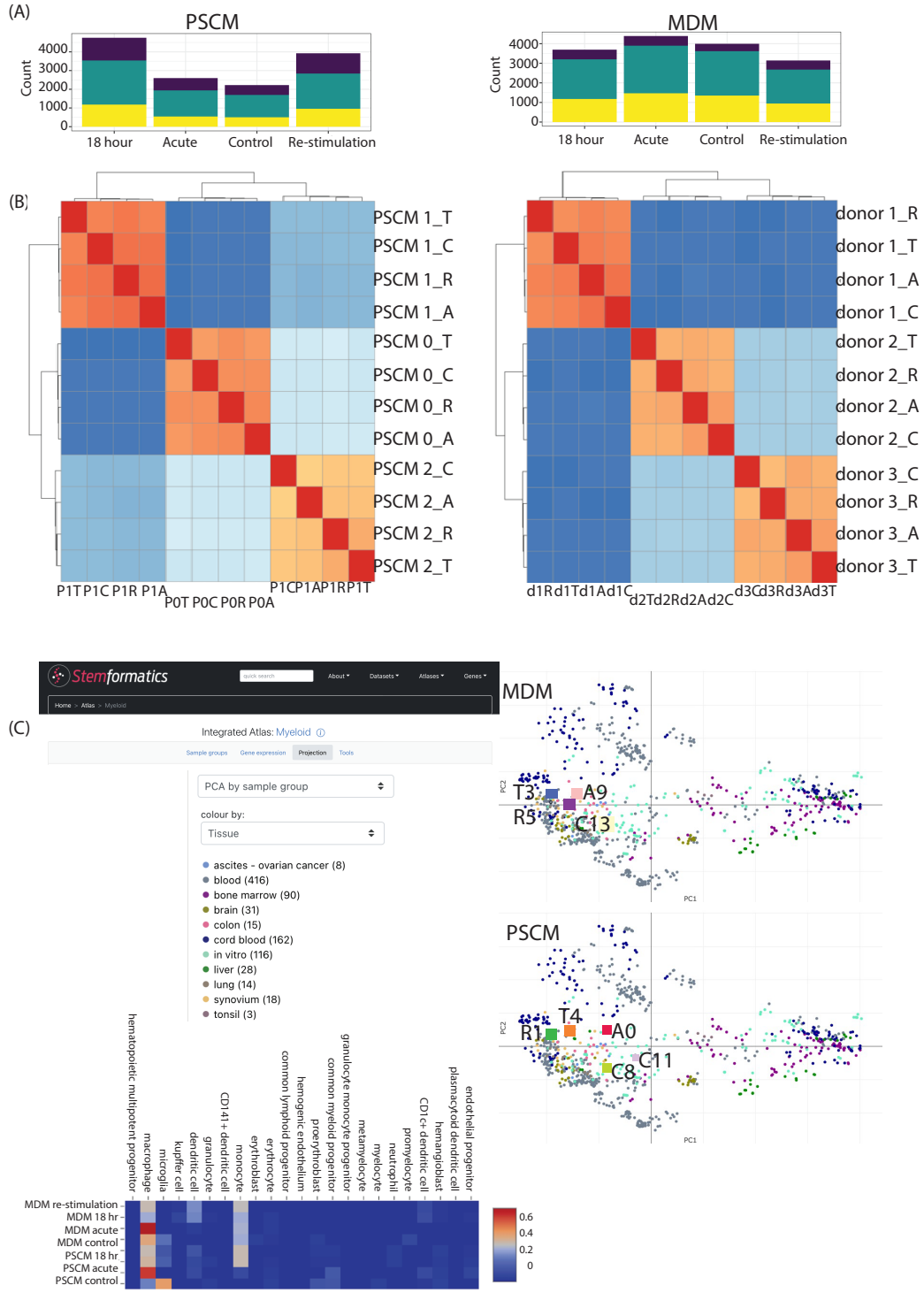

Supplementary Material

Supplementary Table 1: Differential expression analysis of MDM and PSCM groups. Accompanies Figures 1 and 2.

Average and differential expression analysis between MDM and PSCM groups. Average expression, Log2FC, p value, and adjusted p value.

Supplementary Table 2: Average expression of TLR4 signaling components. Accompanies Figure 2A.

Average expression of components of TLR4 signaling pathway. Average expression shown for all identified seurat clusters.